



ASSESSMENT AND COMPARISON OF THE GAMMA AND BC TRANSITION MODELS FOR EXTERNAL FLOWS

Sami KARABAY*, Özgür Uğraş BARAN**

* ROKETSAN A.Ş.06780 Elmadağ, Ankara,

sami.karabay@metu.edu.tr ORCID: 0000-0001-9325-1172

**Orta Doğu Teknik Üniversitesi Makina Mühendisliği Bölümü06800, Ankara,

ubaran@metu.edu.tr ORCID: 0000-0002-8437-7862

(Geliş Tarihi: 04.12.2022, Kabul Tarihi: 23.05.2023)

Abstract: Modelling of transition from the laminar to turbulent flow became a hot topic due to recent developments in renewable energy, UAV technologies and similar aerospace applications. The transition from laminar flow to turbulence is challenging to model in CFD analysis. The drag is overestimated if the transition is neglected in CFD solutions by assuming the flow is fully turbulent. This results in missing the fundamental characteristics of the flow and inaccurate predictions of the flow field. The most popular transition models are Menter's models applied to the SST turbulence model and the Baş-Çakmakçioğlu (BC) transition model applied to the Spalart-Almaras model. We have focused on Menter's simpler but more popular γ model and Baş Çakmakçioğlu models. The γ model relies on the local turbulence intensity, which makes applying the model challenging in external flows. This difficulty stems from the complex relationship between turbulence decay and transition onset. BC transition model utilizes the free stream turbulence intensity. Both models are verified using the Klebanoff and ERCOFTAC flat plate cases and several 2D external flow cases. Skin friction coefficient results are compared to experimental data. Results show that both models predict transition very similarly. BC model is computationally cheaper and easier to implement than the γ model. Also, γ model suffers from boundary conditions ambiguity.

Keywords: Transition Flow, Transition Model, Intermittency, CFD, Flat Plate.

GAMMA VE BC GEÇİŞ MODELLERİNİN DIŞ AKIŞLAR İÇİN DEĞERLENDİRİLMESİ VE KARŞILAŞTIRILMASI

Özet: Laminer akıştan türbülanslı akışa geçişin modelleri, yenilenebilir enerji, İHA teknolojileri ve benzeri havacılık uygulamaları alanındaki son gelişmeler nedeniyle yeniden popüler haline gelmiştir. Laminer akıştan türbülansa geçişin HAD analizlerinde modellenmesi oldukça zor bir konudur. Geçiş bölgesi ihmal edilerek HAD çözümlerinde akışın tamamen türbülanslı olduğu varsayılırsa sürüklenme kuvveti gerçeğinden fazla tahmin edilir. Bu durum, akışın temel özelliklerinin gözden kaçırılmasına ve akış alanının yanlış tahmin edilmesine neden olmaktadır. En popüler geçiş modelleri SST türbülans modeline uygulanan Menter modelleri ve Spalart-Almaras modeline uygulanan Baş-Çakmakçioğlu (BC) modelidir. Bu çalışmada, Menter'in daha sade ama daha popüler olan γ modeli ve Baş Çakmakçioğlu modellerinin dış akışlardaki performansına odaklanılmıştır. γ modeli, harici akışlarda uygulanmasını zorlaştıran yerel türbülans yoğunluğuna dayanmaktadır. Bu zorluk, türbülans azalması ile geçiş başlangıcı arasındaki karmaşık ilişkiden kaynaklanmaktadır. BC geçiş modeli ise serbest akış türbülans yoğunluğunu kullanmaktadır. Her iki model de Klebanoff ve ERCOFTAC düz levha deney verileri ve iki boyutlu harici akış deney verisi kullanılarak doğrulanmıştır. Yüzey sürtünme katsayısı sonuçları deneysel verilerle karşılaştırılır. Sonuçlar, her iki modelin de türbülans geçişini çok benzer şekilde tahmin ettiğini göstermektedir. BC geçiş modeli hesaplama açısından γ modelinden daha ucuz ve uygulaması daha kolaydır. Ayrıca, γ modeli sınır koşullarının pratik olarak belirlenmesindeki belirsizlikten muzdariptir.

Anahtar Kelimeler: Geçişli Akış, Geçiş Modeli, Kesiklilik, HAD, Düz Levha.

INTRODUCTION

The transition from laminar to turbulent regime called laminar-to-turbulent transition, is a complex

and compelling phenomenon in engineering studies. Because of its significant impact on the performance of many real-life applications, including aircraft, wind turbine, and

turbomachinery applications, the laminar-turbulent transition has been the subject of theoretical, experimental, and computational studies. A laminar flow with an ordinary, streamlined velocity profile evolves into a turbulent flow characterized by unpredictable variations in several flow variables. The leap between these very different flow regimes is called turbulence transition. One of the main differences between the laminar and turbulent flows is their very different skin friction. Therefore, transition onset should be modeled to separate these regions for an accurate drag prediction of real-life applications.

The complex nature of transition hinders obtaining accurate predictions of transient flows with an analytic approach. This difficulty leads to new solution methods for turbulence transition using computational fluid dynamics. With the increasing availability of high-performance computing (HPC) resources, there has been a movement in modeling trends toward computations using Large Eddy Simulation (LES) and Direct Numerical Simulation (DNS). Although these numerical approaches have been proven to attain high accuracy, they need a large amount of computing power seldom accessible in everyday simulations. As a result, less resource-intensive techniques, like the RANS methods, remain feasible for general-industrial CFD simulations.

Much effort has been made into numerical modeling of the transition during the last twenty years, resulting in a wide range of methodologies for RANS-based simulations. A family of transition models based on nonlocal variables has been developed in the last two decades. Although they were promising, implementing the nonlocal transition models into general-purpose CFD codes is not practical. Lately, transition models based on local variables have been introduced (Menter et al. (2002), Menter, Langtry et al. (2006), Langtry (2006), Langtry (2006b)).

Transition models use the local variables to attract attention as they can give reasonably accurate solutions. The Langtry-Menter $\gamma - Re_{\theta}$ model (Langtry 2009) is the first approach to modeling transition based on the local variables. The general functionality of the Langtry-Menter $\gamma - Re_{\theta}$ model has increased with additional model modifications to accommodate the effects of surface roughness and crossflow situations. However, this complex model makes it challenging to implement and fine-tune different turbulence models for specific flow scenarios. The Langtry-Menter transition model

also lacks Galilean invariance, an essential property for generic CFD simulations.

Lately, Menter et al. (2015) proposed a new local correlation-based transition model based on a single transport equation and may be thought of as an improved version of the $\gamma - Re_{\theta}$ model. The new model benefits from the simpler formulation. Also, this model is Galilean invariant.

Transition Phenomena

The boundary layer is the flow region adjacent to a bounding surface where viscous effects are significant. The boundary layer has two flow regimes, each with distinct characteristics: laminar and turbulent. Figure 1 depicts a boundary layer development across a plate.

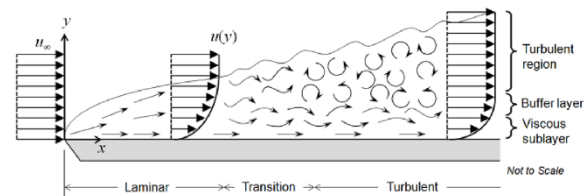


Figure 1. Transition Phenomena Frei, (2013)

When uniform velocity fluid reaches the upstream of the plate, a laminar boundary layer begins to form. The laminar region has a streamlined and smooth velocity profile near the surface. Disturbances in the flow field appear after a certain distance, indicating the onset of the transition zone. The whole flow field ultimately breaks down into a completely turbulent flow characterized by random changes in flow.

The fundamental governing parameter separating viscous flow regions is the Reynolds number that indicates the flow state. It is defined as the ratio of inertial forces to viscous forces. Threshold Reynolds numbers that separate whether the flow is laminar, turbulent, or transition are determined empirically. The point of transition influences the overall properties of the flow. The high velocity gradient in the turbulent boundary layer results in high skin friction than that of the laminar boundary layer. Hence, the total drag of the surface increases. Moreover, laminar and turbulent flows have different heat transfer characteristics besides drag force. Due to the increased mixing in the turbulent flow, significantly higher heat between the fluid and the bounding surface is observed.

On the other hand, determining if the flow is in the transition zone is not straightforward. Unlike the

laminar or fully turbulent zones, the transition flow is unstable. Transitional flow measurements show that a laminar flow is interrupted by turbulent bursts in this zone. Therefore, the flow is split into laminar and turbulent moments. When the Reynolds number is lower, the time spent in laminar periods is larger than in turbulent periods. As the local Reynolds number increases, the time spent in turbulent flow progressively increases, yielding a fully turbulent flow. The percentage of turbulent bursts in total time is called intermittency. The intermittency (γ) is zero when the flow is laminar and one if the flow is fully turbulent. Therefore, intermittency is a key factor in many transition models.

Transition Mechanisms

The transition can occur through different mechanisms due to a variety of reasons. Freestream conditions, turbulence intensity, and surface roughness are examples. Generally, the primary modes are natural, bypass, and separation-induced transitions. Wake-induced and shock-induced transitions are secondary transition modes (Mayle (1991)). In this part, different modes of transition are explained.

Natural Transition: The natural transition is the most common mechanism in low turbulence intensity freestream conditions, as given in Figure 2. In this mechanism, laminar freestream flow reaches critical Reynolds Number Tollmien-Schlichting waves are formed. Then turbulent spots are followed by full turbulent flow (Mayle (1991)). The intermittency increases in the process.

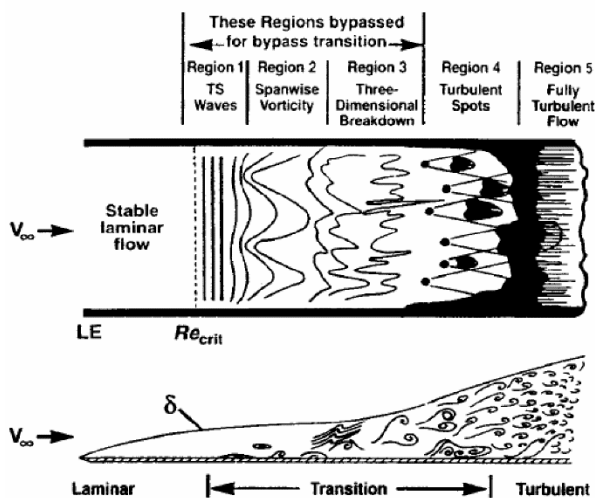


Figure 2. Natural Transition Mode Frei, (2013)

Bypass Transition: If the freestream turbulence level is larger than 1%, natural transition stages are

bypassed, and turbulent spots are produced directly. In this mode, linear stability theory fails, and no Tollmien-Schlichting waves are formed. Freestream turbulence level, rough surface, and favorable pressure gradients can also be reasons for the bypass transition mode.

Separation-Induced Transition: The transition may occur in the shear layer when the flow separates. In this mode, a laminar separation bubble can be formed on the surface, resulting in the flow reattachment. This mode contains all stages of the natural transition. According to the freestream turbulence level, the size of the separation bubble changes.

Wake-Induced Transition: This transition mode can be observed on periodic unsteady turbulent wakes passing over blades or airfoils (Langtry (2006), Wang (2021)). Turbulent wakes disrupt the laminar boundary layer when they impinge the wakes, and turbulent spots propagate downstream.

Reverse Transition: Reverse transition or relaminarization refers to the transition from turbulent to laminar

Transition Modelling

It is possible to consider transition models according to their level of sophistication. The most basic model is the e^N model from Smith (1956). The model is applied to a 2D steady flow by Nichols (2010), and it is based on the linear stability theory and is often used for low-turbulence flows. A velocity profile is required a priori.

More advanced low Reynolds Number turbulence models were introduced by Jones (1973). These models modify wall-damping functions to capture the transition effects. These models rely on turbulence diffusion from the freestream into the boundary layer to anticipate the transition onset. Low Reynolds Number turbulence models are generally used for bypass transition flows. However, they are unreliable since they are not sensitive to pressure gradients and flow separations (Dhawan (1958)).

Next, a group of more advanced and complex transition models called correlation-based transition models were formulated by Kaynak et al. (2019). The main idea is to blend the laminar and turbulent regions by introducing a new variable, intermittency (Langtry (2009)). Intermittency could be defined as the probability that the flow is

turbulent. These models try to model the intermittent character of turbulence resulting from the fluctuations in the flow field. A new set of algebraic or partial differential equations are coupled with existing turbulence models Such as Langtry (2009), Suzen (2006), Walters (2008) and Çakmakçioğlu (2018). In those equations, constants derived from experiments and observations are used. It is convenient to group these models according to whether they use local or nonlocal flow variables.

Models Depending on Nonlocal Flow Variables

The transition mechanism and the Momentum Reynolds number are proven experimentally correlated. The momentum thickness Reynolds number is the Reynolds number based on the momentum thickness, θ .

$$Re_{\theta} = \frac{\rho U_e \theta}{\mu} \quad (1)$$

Experimental correlations reveal that the transition onset is observed at a critical momentum thickness Reynolds number, $Re_{\theta c}$. Many models are based on this correlation. Note that $Re_{\theta c}$ is not a local parameter and should be calculated starting from the wall. Therefore these models need to use an exhausting search algorithm to calculate the momentum thickness Reynolds number for complex flows. For example, The Dhawan and Narasimha (1958) model is the first attempt at correlation-based transition models. They proposed an algebraic intermittency function (γ) assuming the transition onset, (x_t), is known as a priori.

Steelant and Dick (2001) proposed a set of transport equations called the conditional Navier- Stokes equations. Their transport equation is derived from the intermittency function proposed by Dhawan and Narasimha. The model can predict intermittency in the streamwise direction by assuming uniform intermittency distribution in the cross-stream direction. However, their approach is not consistent with experimental data.

Cho and Chung (1992) proposed a new transport equation coupled with the $k - \varepsilon$ turbulence model. The model itself cannot predict the onset of transition. However, intermittency profiles agree with the experimental results for various flow conditions.

Suzen and Huang (2000) improved the intermittency equation approach significantly.

Their intermittency transport equation includes source terms from the Steelant and Dick and Cho-Chung models. The transport equation is coupled with Menter's (1994) shear stress transport turbulence model. The model's superiority is that the intermittency profile along the cross-stream direction can be predicted, which was the shortcoming of the previous models.

Models Depending on Local Flow Variables

These models use constants derived from observations and experiments in transport equations. A prominent feature of these models is that they are compatible with modern CFD codes as vorticity Reynolds Number is used. Re_V is calculated as follows;

$$Re_V = \frac{\rho d_w^2}{\mu} \Omega \quad (2)$$

In Equation (2), d_w denotes the distance from the nearest wall. Since all variables used are local, Re_V is also a local variable that can be computed in CFD codes. The Blasius theory shows that the local vorticity Reynolds Number, Re_V , is proportional to the momentum thickness Reynolds Number, Re_{θ} , which is a fundamental parameter for transition. Thus, local correlation transition models can be used to model transition in CFD simulations.

The first of these models proposed by Langtry (2009) and Menter is the $\gamma - (Re_{\theta t})$ model. Two additional scalar transport equations (3)-(4) are solved besides the SST model transport equations.

$$\frac{\partial(\rho\gamma)}{\partial t} + \frac{\partial(\rho u_j \gamma)}{\partial x_j} = P_{\gamma} - E_{\gamma} + \frac{\partial}{\partial x_j} \left[\left(\mu + \frac{\mu_t}{\sigma_f} \right) \frac{\partial \gamma}{\partial x_j} \right] \quad (3)$$

$$\frac{\partial(\rho \hat{R}e_{\theta t})}{\partial t} + \frac{\partial(\rho u_j \hat{R}e_{\theta t})}{\partial x_j} = P_{\theta t} + \frac{\partial}{\partial x_j} \left[\sigma_{\theta t} (\mu + \mu_t) \frac{\partial \hat{R}e_{\theta t}}{\partial x_j} \right] \quad (4)$$

The first of these two equations is for intermittency (γ). The second one solves for transition momentum thickness Reynolds Number ($Re_{\theta t}$), which refers to a local Re_{θ} . Menter's $\gamma - (Re_{\theta t})$ model formulation consists of local variables. Hence, it can be used for complex flows with any grid type.

Menter (2015) proposed the simplified version of the $\gamma - (Re_{\theta t})$ model. In the new model, called

Menter's one equation γ model, the $(Re_{\theta t})$ transport equation is removed, and experimental correlations are embedded into the intermittency equation. The transport equation is the same as the $\gamma - (Re_{\theta t})$ model transport equation, as given in (5). However, source terms are slightly modified, and some constants differ.

$$\frac{\partial(\rho\gamma)}{\partial t} + \frac{\partial(\rho u_j \gamma)}{\partial x_j} = P_\gamma - E_\gamma + \frac{\partial}{\partial x_j} \left[\left(\mu + \frac{\mu_t}{\sigma_f} \right) \frac{\partial \gamma}{\partial x_j} \right] \quad (5)$$

Although one of the equations is removed, the new model provides good predictions. The main advantage of the γ model is that it solves one less equation than the previous model.

Another local correlation-based transition model is the Walters-Cokljat (2008) $k_T - k_L - \omega$ model. This model is based on the concept that the cause of the bypass transition is very high amplitude streamwise fluctuations. These fluctuations differ from turbulent fluctuations and can be modeled separately. Mayle and Schulz (1996) proposed a second kinetic energy equation to describe these fluctuations. This kinetic energy was called laminar kinetic energy k_L . In this model, total kinetic energy is assumed to be the sum of the energy of large-scale and small-scale eddies. Large-scale eddies contribute to laminar kinetic energy, and small-scale eddies contribute to turbulent kinetic energy production. Thus, the transition can be modeled by calculating the k_L , with the transport equation given in (6). Besides the merely changed $k - \omega$ transport equations, one more transport equation is solved to calculate laminar kinetic energy.

$$\frac{Dk_L}{Dt} = P_{k_L} - R_{BP} - R_{NAT} - D_L + \frac{\partial}{\partial x_j} \left[\nu \frac{\partial k_L}{\partial x_j} \right] \quad (6)$$

Since this model uses local formulation, it can be used in CFD codes.

The last model mentioned is Bas-Cakmakcioglu (2018) (BC) algebraic transition model. This model solves one algebraic equation instead of a partial differential equation for intermittency. Therefore, the computational cost of CFD simulations reduces significantly. BC transition model damps the turbulent production term of the Spalart-Allmaras (S-A) turbulence mode until the transition onset threshold is reached. Lately, the model has become

Galilean invariant with modification in the formulation (2013, Çakmakçioğlu (2020)). Also, the local Reynolds number, hence the reference length, dependency of the original method is corrected. Thus, the BC algebraic transition model can be used for various flows with any grid type without the reliance on reference length selection.

The recent years Menter's γ model has gained significant popularity due to its popularity in commercial solvers. On the other hand, the BC transition model became available on open-source CFD code SU^2 solver. No widely available open-source solver allows the comparison of these models. Such comparison is necessary to eliminate the effects of the flow solver scheme. In this study, we aim to implement both models in the same solver and clearly compare these transition models.

METHODOLOGY

This section describes the implemented transition models. Also, the mesh domain used in simulations is elaborated on in this section.

Transition Prediction

A transition model should predict the onset and length of the transition. Transition length and characteristics are controlled by the intermittency concept, which refers to the probability of a point being in a turbulent region Emmons (1951))

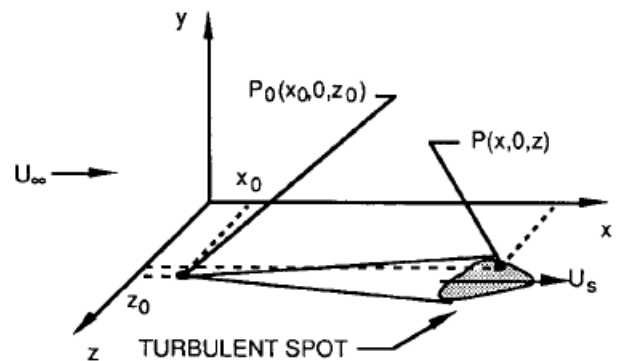


Figure 3: Intermittency in Space, Mayle (1991)

Intermittency equals one if in the fully turbulent boundary. If the flow is laminar, the intermittency is zero. Intermittency can be modeled with an algebraic function or with a transport equation. Source terms of the transport equations are responsible for the algebraic transition models in these equations. Modeling intermittency with the transport equation provides the modeling transition across the boundary layer and in the streamwise

direction. Thus, this approach gives more accurate solutions than the algebraic approaches.

The task of intermittency is to control the transition characteristics and length of the transition. As the boundary layer develops, intermittency, γ , increases and eventually, it becomes equal to unity. From this point on, the transition phase is completed, and the flow becomes fully turbulent. The underlying turbulence model is employed for turbulent flow. However, another mechanism besides intermittency is required to predict the onset of the transition.

Prediction of Transition Onset

Momentum thickness Reynolds number is a flow parameter that is calculated using the momentum given in the previous section. Transition onset momentum thickness Reynolds number, Re_{θ_t} , is the momentum thickness Reynolds number calculated at transition onset.

Studies and experiments show that transition onset is strongly related to the free stream turbulence intensity and pressure gradient. Experiments have shown that transition onset is earlier as turbulent intensity increases and transition onset momentum thickness Reynolds Number, Re_{θ_t} , gets smaller, as shown in Figure 4.

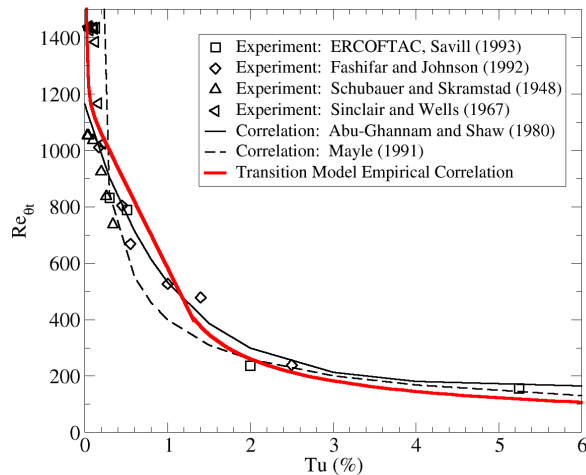


Figure 4: Relation between the Turbulence Intensity and Transition Onset Momentum Thickness Reynolds Number (Menter (2006b))

Thus, a transition model should include the effect of turbulence intensity. Menter's (2015) one-equation γ model utilizes the local turbulence intensity to provide a measure of intermittency. Then the term $(1 - \gamma)$ is multiplied by the turbulence production term to prevent or limit turbulence production near the wall.

The pressure gradient is decisive for the transition onset, similar to turbulence intensity. As shown in Figure 5, the transition onset momentum thickness Reynolds number decreases with increasing turbulence intensity. In other words, transition onset delays with a larger pressure gradient in the boundary layer.

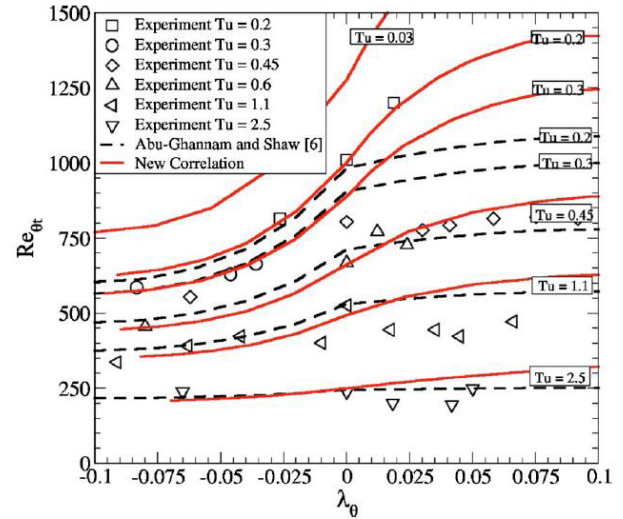


Figure 5: Relation between the Pressure Gradient Parameter and Transition Onset Momentum Thickness Reynolds Number (Menter (2006b))

To include the effect of the pressure gradient, the transition onset is calculated using the pressure gradient parameter term, λ_θ , besides the turbulent intensity. This term is also calculated from the local streamwise acceleration.

MENTER ONE-EQUATION γ MODEL

Menter's one-equation γ model is a simplified version of their γ -(Re_{θ_t}) model. The difference is that the former does not solve any transport equation for momentum thickness Reynolds number, (Re_{θ_t}), but it is computed algebraically using local variables in the intermittency transport equation.

Menter (1994) implemented one equation γ model on the $k-\omega$ SST. The new model is calibrated with available experimental data. Calibration is done for self-similar flows, Falkner-Skan family flows and some non-equilibrium flows, mainly with separation. The adjustment of the model coefficients conducted according to self-similar flows and separation results with some differences with experimental data for different transition mechanisms.

The novelty of the Menter one-equation γ model is that, unlike turbulence models, this model does not seek to represent the physics of the transition process but rather provides a framework for incorporating correlation-based models into general-purpose CFD codes. The physics of the transition phenomenon is contained in the model's empirical correlations. As a result, this formulation is not confined to a single transition mechanism, such as natural transition or bypass transition. The formulation can be applied to any transition mode as long as modifications of the correlations are embedded into the model coefficients.

Menter's Transition Model

The intermittency transport equation of the Menter one equation γ model is presented in Equation (7).

$$\frac{\partial(\rho\gamma)}{\partial t} + \frac{\partial(\rho U_j\gamma)}{\partial x_j} = P_\gamma - E_\gamma + \frac{\partial}{\partial x_j} \left[\left(\mu + \frac{\mu_t}{\sigma_f} \right) \frac{\partial \gamma}{\partial x_j} \right] \quad (7)$$

The γ production term is defined as:

$$P_\gamma = F_{length} \rho S \gamma (1 - \gamma) F_{onset} \quad (8)$$

In equation 4-(8), S refers to the strain rate magnitude. It is included in the production term as a multiplier, as strain rate is the driving factor of the transition process. F_{length} is a calibration constant. F_{onset} is the term that triggers the onset of the transition. This term involves the ratio of vorticity Reynolds number to critical Reynolds number, between which a strong relationship is shown experimentally.

Before the onset of the transition, where flow is laminar, the production term is equal to zero, as expected. The destruction term in the transport equation is as follows:

$$E_\gamma = c_{a2} \rho \Omega \gamma F_{turb} (c_{e2} \gamma - 1) \quad (9)$$

Constants used in the production and destruction terms are given below.

$$F_{length} = 100, c_{e2} = 50, c_{a2} = 0.06, \sigma_\gamma = 1.0, \quad (10)$$

Functions used in calculating the production and destruction terms are given below.

$$\begin{aligned} F_{onset1} &= \frac{Re_\gamma}{2.2 Re_{\theta c}}, \\ F_{onset2} &= \min(F_{onset1}, 2.0), \\ F_{onset3} &= \max\left(1 - \left[\frac{R_T}{3.5}\right]^3, 0\right), \\ F_{onset} &= \max(F_{onset2} - F_{onset3}, 0), \\ F_{turb} &= e^{-\left(\frac{R_T}{4}\right)^2}, R_T = \frac{\rho k}{\mu \omega}, \\ Re_\gamma &= \frac{\rho d_\omega^2 S}{\mu}, Re_{\theta c} = f(Tu_L, \lambda_{\theta L}) \end{aligned} \quad (11)$$

The boundary conditions of the transport γ -model are that flux of the γ through the wall is zero, and γ equals unity at the inlet to preserve the freestream turbulence decay rate of the underlying turbulence model (Langtry (2009)).

The critical momentum thickness Reynolds number, $Re_{\theta c}$, is defined as a function of the local turbulent intensity and pressure gradient parameter. Thus, to calculate $Re_{\theta c}$, local turbulent intensity and local pressure gradient parameters are calculated. Local turbulent intensity, Tu_L , is defined as:

$$Tu_L = \min\left(\frac{100\sqrt{2k/3}}{\omega d_\omega}, 100\right) \quad (12)$$

This formulation allows the local turbulent intensity to equal the freestream turbulent intensity in the middle of the boundary layer. The pressure gradient parameter is defined as follows:

$$\lambda_{\theta L} = -7.57 \times 10^{-3} \frac{dV}{dy} \frac{d_\omega^2}{\nu} + 0.0128 \quad (13)$$

Coefficients in this formula are selected considering the self-similar flows. To achieve numerical robustness, Menter bounded $\lambda_{\theta L}$ as follows:

$$\lambda_{\theta L} = \min(\max(\lambda_{\theta L}, -1.0), 1.0) \quad (14)$$

Coupling with SST Turbulence Model

The coupling of the Menter one equation γ model with the SST turbulence model is done by slightly modifying the transport original transport equations of turbulent kinetic energy (Menter (2015))

$$\begin{aligned}
\frac{\partial}{\partial t}(\rho k) + \frac{\partial}{\partial x_j}(\rho u_j k) = & \\
& \tilde{P}_k + P_k^{\text{lim}} - \tilde{D}_k + \frac{\partial}{\partial x_j} \left[(\mu + \sigma_k \mu_t) \frac{\partial k}{\partial x_j} \right] \\
\frac{\partial}{\partial t}(\rho \omega) + \frac{\partial}{\partial x_j}(\rho u_j \omega) = & \alpha \frac{P_k}{\nu_t} - D_\omega \\
& + CD_\omega + \frac{\partial}{\partial x_j} \left[(\mu + \sigma_\omega \mu_t) \frac{\partial \omega}{\partial x_j} \right]
\end{aligned} \quad (15)$$

Also:

$$\begin{aligned}
\tilde{P}_\gamma &= \gamma P_k \\
\tilde{D}_\gamma &= \max(\gamma, 0.1) D_k
\end{aligned} \quad (16)$$

Where P_k and D_k are the production and destruction terms of the original turbulent kinetic energy of the equation of SST. The updated k equation includes the term P_k^{lim} to provide the generation of k at the transition phase for small turbulence intensity values.

$$\begin{aligned}
P_k^{\text{lim}} &= 5C_k \max(\gamma - 0.2, 0) \\
& (1 - \gamma) F_{on}^{\text{lim}} \max(3C_{sep}\mu - \mu_t, 0) S\Omega \\
F_{on}^{\text{lim}} &= \min \left(\max \left(\frac{Re_\nu}{2.2Re_c^{\text{lim}}} - 1, 0 \right), 3 \right) \\
Re_{\theta c}^{\text{lim}} &= 1100, c_k = 1.0, c_{sep} = 1.0
\end{aligned} \quad (17)$$

BC Transition Model

The BC transition model relies on the experimental correlation of the transition location and the theoretical relation between $Re_{\theta c}$ and $Re_{\nu, max}$. The critical momentum thickness is given in equation (18) based on experimental data.

$$Re_{\theta c} = 803.73(Tu_\infty + 0.6067)^{-1.2027} \quad (18)$$

The above equation provides an excellent theoretical basis for the transition onset. Equation (18) correlates the free stream turbulence intensity and the transition onset rather than the local turbulence intensity as Menter's model does. Indeed, no correlation for the latter case is available in the literature.

The parameter $Re_{\theta c}$ is utilized to determine the intermittency.

$$\begin{aligned}
\gamma_{BC} &= 1 - \exp(-\sqrt{\text{Term1}} - \sqrt{\text{Term2}}) \\
\text{Term1} &= \frac{\max(Re_\theta - Re_{\theta c}, 0.0)}{\chi_1 Re_{\theta c}} \\
\text{Term2} &= \frac{\max(\gamma_{BC} - \chi_2, 0.0)}{\chi_2}
\end{aligned} \quad (19)$$

Finally, the Spalart-Almaras turbulence model is modified to Equation (20). The only difference from the original equation is the multiplication of the production term with γ_{BC} , as indicated by the boldface. Therefore, the turbulence equation does not alter where the intermittency is equal to one.

$$\begin{aligned}
\frac{\partial}{\partial t}(v_T) + \frac{\partial}{\partial x_j}(u_j v_T) = & \\
& \boldsymbol{\gamma}_{BC} C_{b1} S v_T - c_{w1} f_w \left(\frac{v_T}{d_w} \right)^2 \\
& + \frac{1}{\sigma} \left\{ \frac{\partial}{\partial x_j} \left[(\nu_L + \nu_T) \frac{\partial v_T}{\partial x_j} \right] - C_{b2} \frac{\partial v_T}{\partial x_j} \frac{\partial v_T}{\partial x_j} \right\}
\end{aligned} \quad (20)$$

COMPUTATIONAL SETUP VALIDATION

In this section, we have validated our solver and our γ model implementations. The transition model verification is conducted by comparing our results with the reference (Menter (2015)) implementations. Also, we have shown the mesh study in this section. The validated meshing strategy is repeated for flat plate verification studies.

CFD Solver

All developments are implemented in our cell-based finite volume solver. The current $k - \omega - \gamma$ development is applied as a new turbulent solver library starting from the $k - \omega$ model. All the necessary modifications are done, and changes to the SST model are implemented. The Bař-Çakmakçiođlu model, however, is added directly to the SA solver. We have utilized their (2020) model, as this model provides the Galilean invariance and Reynolds number independence. The applied flux scheme is the second-order accurate implicit HLLC with Venkatakrisnan limiter. The solver and turbulence models are validated in previous studies (Dikbař (2022), Duru (2021)).

Experimental Data for Transition

The number of available test cases utilized for transition modeling is somewhat limited. We have used the standard flat plate test cases and some 2D test cases.

Flat Plate Cases

Standard benchmark cases to test the development and implementation of transition models are available in the literature. Those are Schubauer-

Klebanoff (1955) and ERCOFTAC series experiments.

The Schubauer-Klebanoff (1955) flat plate test case is one of the most well-known flat plate cases used to validate transition models. This test is a natural transition on a flat plate with low freestream turbulence intensity. This test case

The T3 experiments were conducted by Rolls Royce in the 1990s and have become benchmark cases for transition model validation by Savill et al. (1993). The bypass transition mode dominates the transition in all T3 cases due to high freestream turbulence intensities. Freestream velocity profiles, freestream turbulence intensity profiles and skin friction coefficients are measured and reported in the T3 series. T3A, T3B and T3A- are zero-pressure gradient flat plate cases. T3C series are nonzero pressure gradient cases.

All flat plate test conditions are given in Table 1. Note that turbulent viscosity is taken from Menter's study. BC transition model does not require this ratio.

One notable difference between Menter's study and experimental data appears in the Schubauer Klebanoff test case. Schubauer and Klebanoff conducted their experiments at a free stream velocity of 80 ft/s, which is changed to 50.1 m/s in Menter's study. S&K experiment reports that the transition occurs at x-locations between 5 to 8 inches. Menter reported wall shear stress results, first as local Reynolds number, then x locations. Both results are consistent with the experiments in terms of Reynolds numbers, where the transition Reynolds number is around 3×10^6 . There is an ambiguity in the free stream turbulence level, too. Schubauer reports the free stream turbulence as 0.03%. Menter reports this value at 0.3% in Table 1 and 0.18% in Figure 4 in their 2009 study, and 0.03% in their 2015 study. Indeed, the free stream turbulence level is very low, and either selection has no significant effect on the results.

Table 1: Inlet Conditions of Different Test Cases

Case	U in [m/s]	Tu (%)	μ_t/μ	ρ , kg/ m ³	μ , kg/ms
S&K	50.1	0.18	1	1.2	1.8×10^{-5}
T3A	5.18	4.5	8	1.2	1.8×10^{-5}
T3B	9.4	7.8	80	1.2	1.8×10^{-5}
T3A-	19.8	1.1	6	1.2	1.8×10^{-5}

T3C2	5.4	3	9	1.2	1.8×10^{-5}
T3C3	4.0	3	5	1.2	1.8×10^{-5}
T3C4	1.4	3	2	1.2	1.8×10^{-5}
T3C5	9.1	7	12	1.2	1.8×10^{-5}

Mesh Generation

It is shown that the $(\gamma - Re_{\theta t})$ and Menter one equation γ model is sensitive to mesh properties both streamwise and normal to wall directions. Menter et al. (2015) recommend following practice rules in mesh generation for Menter one equation γ model;

- Dimensionless wall distance y^+ should be less than one,
- The expansion ratio in the normal wall direction should be less than 1.1,
- At least 30 cells normal to wall direction,
- At least 100 cells in a streamwise direction.

The grid convergence studies for all cases are conducted, and one study is presented for the Schubauer-Klebanoff case. Five different meshes with different numbers of cells are created, considering the guidelines mentioned above. The convergence plot based on the drag is given in Figure 6. The x-axis represents the $(1/N)^{1/2}$, which is proportional to average grid spacing, h . Labels indicate the normal to wall mesh and (×) streamwise mesh counts.

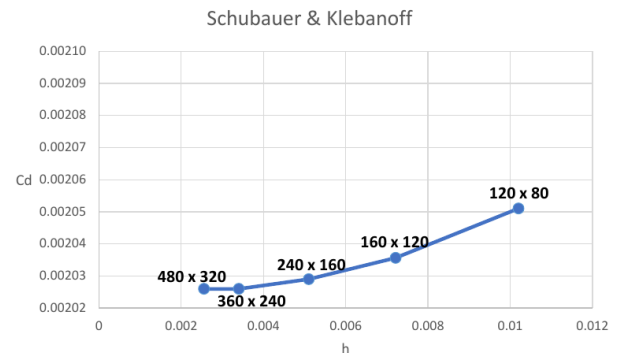


Figure 6: Convergence of Drag coefficient

Skin friction coefficients obtained using five grids are reported in Figure 7. Computational skin frictions are calculated the wall boundaries that are shown in red in Figure 8. The experimental data is taken from Schubauer Klebanoff study. The experimental measurement locations are correlated through Reynolds similarity.

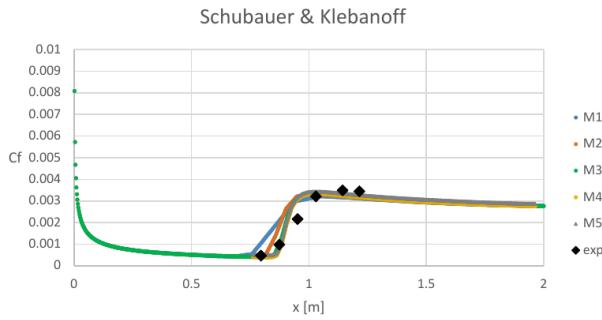


Figure 7: Skin friction coefficients obtained using five meshes

Similar to the drag coefficient, skin friction coefficients converge as the element size in the streamwise direction decreases. We have followed a similar approach for all test cases. The mesh independence studies of the other cases are not involved in this study.

The properties of the meshes used are presented in Table 2.

Table 2: Mesh Properties

Case	Cells	Expansion Ratio	First Cell Thickness	y^+
Zero Pressure Gradient	240×160×1	1.08	2x10 ⁻⁵	0.8
Nonzero Pressure Gradient	255×150×1	1.05	1x10 ⁻⁵	0.7

Computational Domain

Boundary conditions assigned to mesh obtained at the end of the mesh generation process are shown in Figure 8.

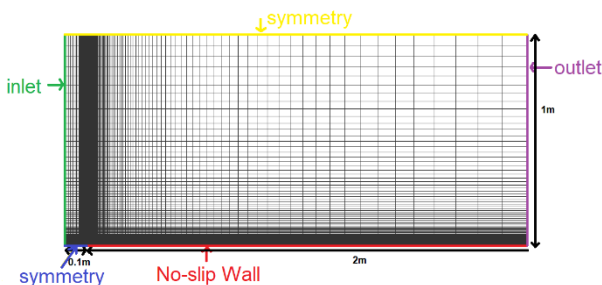


Figure 8: Computational Domain for Zero Pressure Gradient Cases

At the inlet, velocity, pressure and density are specified with turbulent kinetic energy k and dissipation rate, ω . Very high-quality and dense mesh is defined at the leading edge of the flat plate to resolve the stagnation point with reasonable

accuracy. y^+ is kept close to unity. The Klebanoff, T3A, T3B and T3A- test cases are solved using the mesh explained.

T3C series are the cases with pressure gradients. The computational domain of T3C cases is generated in the converging-diverging duct form to simulate the pressure gradient.

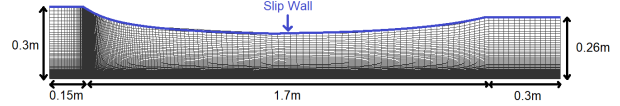


Figure 9: Mesh Domain for Cases with Pressure Gradient

RESULTS

Simulation results are compared with experimental data in this section, and comments are given. We have verified our flat plate solutions with Menter's solutions (2015) to eliminate implementation errors in our conclusions. Therefore, the flat plate cases serve for both implementation validation and model comparison purposes.

Flat plate results

Schubauer-Klebanoff Test Case

Results of the Schubauer-Klebanoff test case show that Menter one equation γ model and the Bas-Cakmakcioglu model can predict natural transition accurately. Bas-Cakmakcioglu model predicts skin friction coefficient better than the Menter one-equation γ model after the flow becomes fully turbulent for the Schubauer-Klebanoff test case. Menter's reported solution taken from the 2015 study is also given in Figure 10. The turbulence decay is not reported for this experiment. The experimental data shows the transition onset is around $Re_x = 3 \times 10^6$ ($x = 0.8$ in our case). The transition length extends the transition zone until $x=1.2$. The BC transition model is an abrupt transition model that does not incorporate the transition length. The sudden jump from the laminar to turbulent flow is visible in Figure 10. The γ model claimed to be calibrated for the transition length. However, the γ solution shows abrupt (or short-length) transitions like BC Model. This observation was repeated for other flat plate test cases.

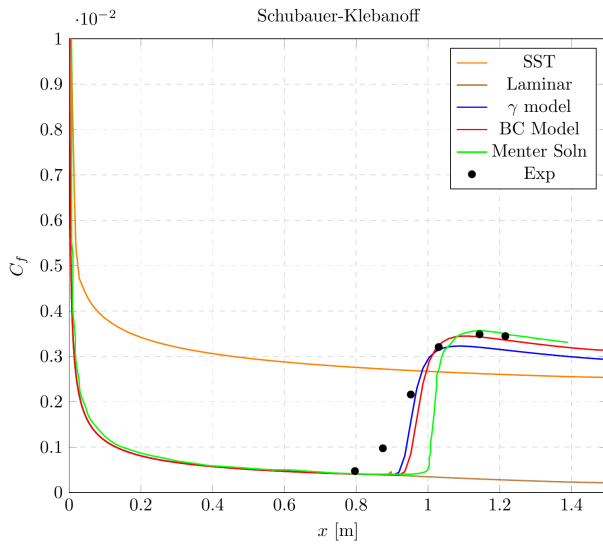


Figure 10: Comparison of Skin Friction Coefficients obtained with Different Models, including Menter's (2015) results for S&K Case

ERCOFTAC Zero Pressure Gradient Cases

T3A, T3B and T3A- zero pressure gradient cases are examined with the studied transition models. These cases are more challenging than the S&K case since they are bypass transition cases as turbulent intensities are larger than 1% or close to 1%. Thus, resolving the transition in these cases is more challenging than in the S&K case. The inlet freestream turbulence intensity and viscosity ratio are adjusted according to experimental turbulence intensity data. Turbulence intensity profiles and skin friction coefficients are given in the following figures. We have compared our results with the Menter (2015) study in these figures. Other solutions are obtained from our solver.

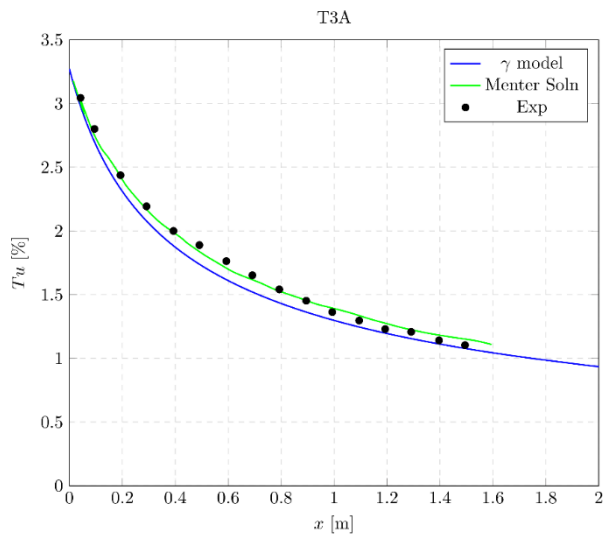


Figure 11: Turbulence intensity profile of T3A simulation

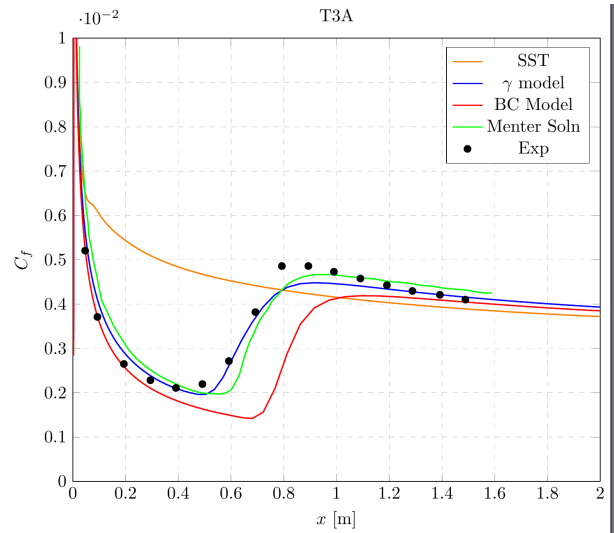


Figure 12: Comparison of Skin Friction Coefficients obtained with Different Models for T3A Case

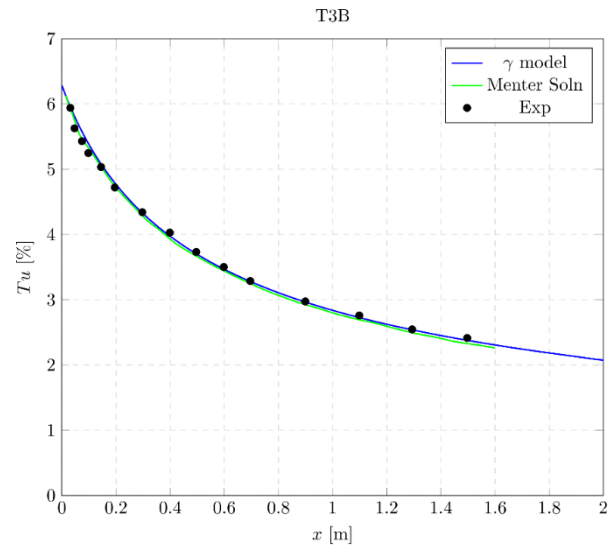


Figure 13: Turbulence intensity profile of T3B simulation

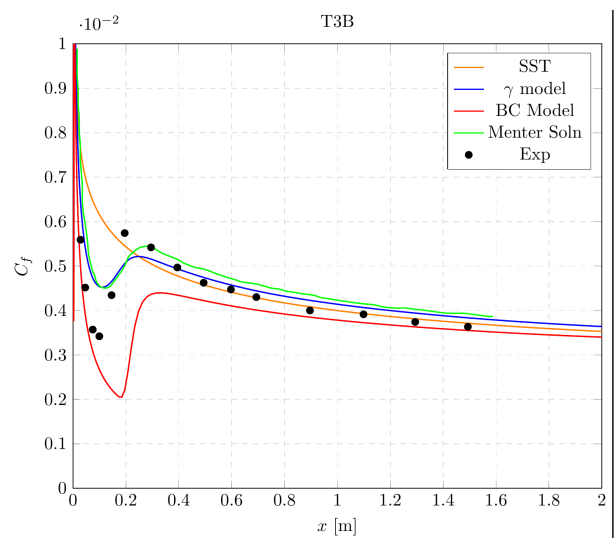


Figure 14: Comparison of Skin Friction Coefficients obtained with Different Models for T3B Case

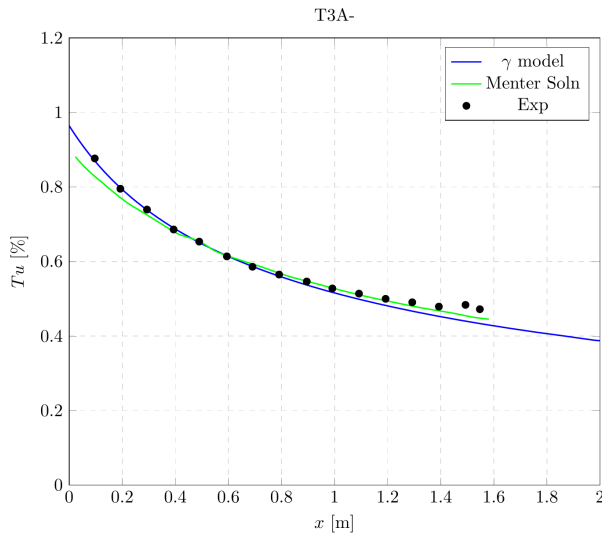


Figure 15: Turbulence intensity profile of T3A-simulation

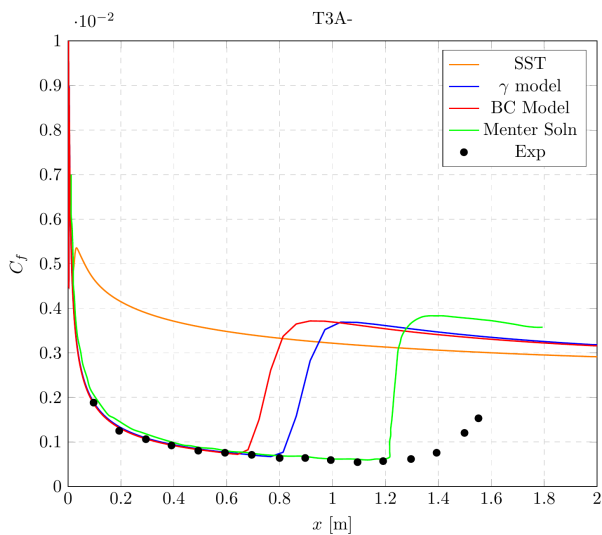


Figure 16: Comparison of Skin Friction Coefficients obtained with Different Models for T3A- Case

Menter's solutions are digitized from the original (2015) paper and added to T3A and T3B plots to show that the model is implemented correctly. The small discrepancy between Menter's results and obtained results during this study could be the difference in flux schemes between the two codes. Nevertheless, the results match well.

Menter's one-equation γ model performed better than the BC transition model for the T3A case. The flow becomes fully turbulent in the T3B case immediately after interacting with the flat plate. The γ and BC transition models have captured transition with reasonable accuracy. The challenging aspect of T3A- is that transition onset occurs at the end of the plate. None of the transition models could predict transition onset correctly.

We should highlight a few important points in some ERCOFTAC cases. The validation cases involve some extreme conditions that make the model validation challenging. The T3B case features extremely high freestream turbulence intensity. Therefore, the transition occurs almost immediately. This feature makes the tuning of the γ model very difficult for this extreme case. A similar observation is valid for the BC transition model. This extreme case is particularly important in practice since the laminar flow section is short, and drag estimations are not affected significantly by the application of a transition model. In practice, this test case is very close to fully turbulent flows and a classical turbulence model can be utilized.

Finally, the shortcomings of a transition-free turbulence model should also be mentioned. We have employed $k - \omega - SST$ turbulence model for this purpose since it constitutes the basis of γ model. As seen from Figures 10, 12, 14 and 16, the original $k - \omega - SST$ model underestimates the skin friction at the fully turbulent zone. The mismatch is more significant when the free stream turbulence is low and the transition length is short. A similar observation is reported between SA and SA-BC models.

Results for ERCOFTAC Nonzero Pressure Gradient Cases

The ERCOFTAC test cases T3C2, T3C3, T3C4 and T3C5 are used to validate the model in the scenario of a transitional boundary layer with the influence of a pressure gradient. The favorable pressure gradients impact the transition onsets of T3C2, T3C3, T3C4 and T3C5 under various freestream velocity changes. Analyses are done using The Menter one-equation γ and BC transition models. The results obtained in this section are highly dependent on computational domains. As mentioned, the pressure gradient is implemented using the converging-diverging duct shape domain. The upper boundary should be generated to satisfy the experimental data of local free stream flow velocity. The computational domain is obtained iteratively. The same domain is used for all T3C simulations. Inlet turbulence intensity and viscosity ratios are assigned considering turbulence intensity profiles of experimental data. Velocity profiles obtained using the inlet conditions in Table 1 are given in Figure 17 for T3C cases.

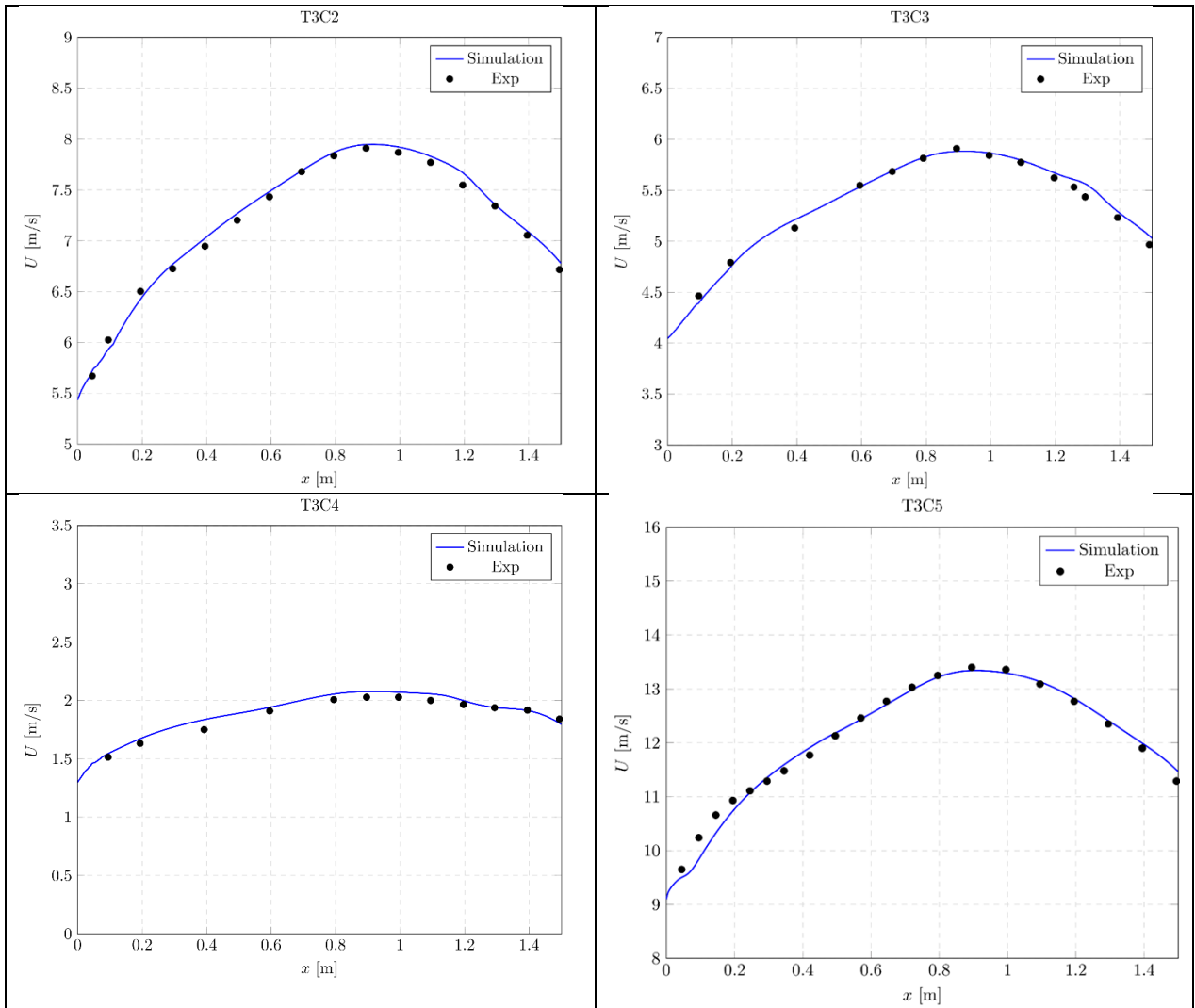


Figure 17: Distributions of freestream velocity for T3C cases. The freestream velocities are taken from the last velocity readings at each x-stations from experimental data. The numerical data is taken through a curve passing the same (x,y) locations and obtained with the γ model.

Velocity profiles reasonably agree with the experimental data. Turbulence intensity profiles of the simulations are presented in Figure 18. This

proves that the geometry generated for turbulence dat work reasonably well.

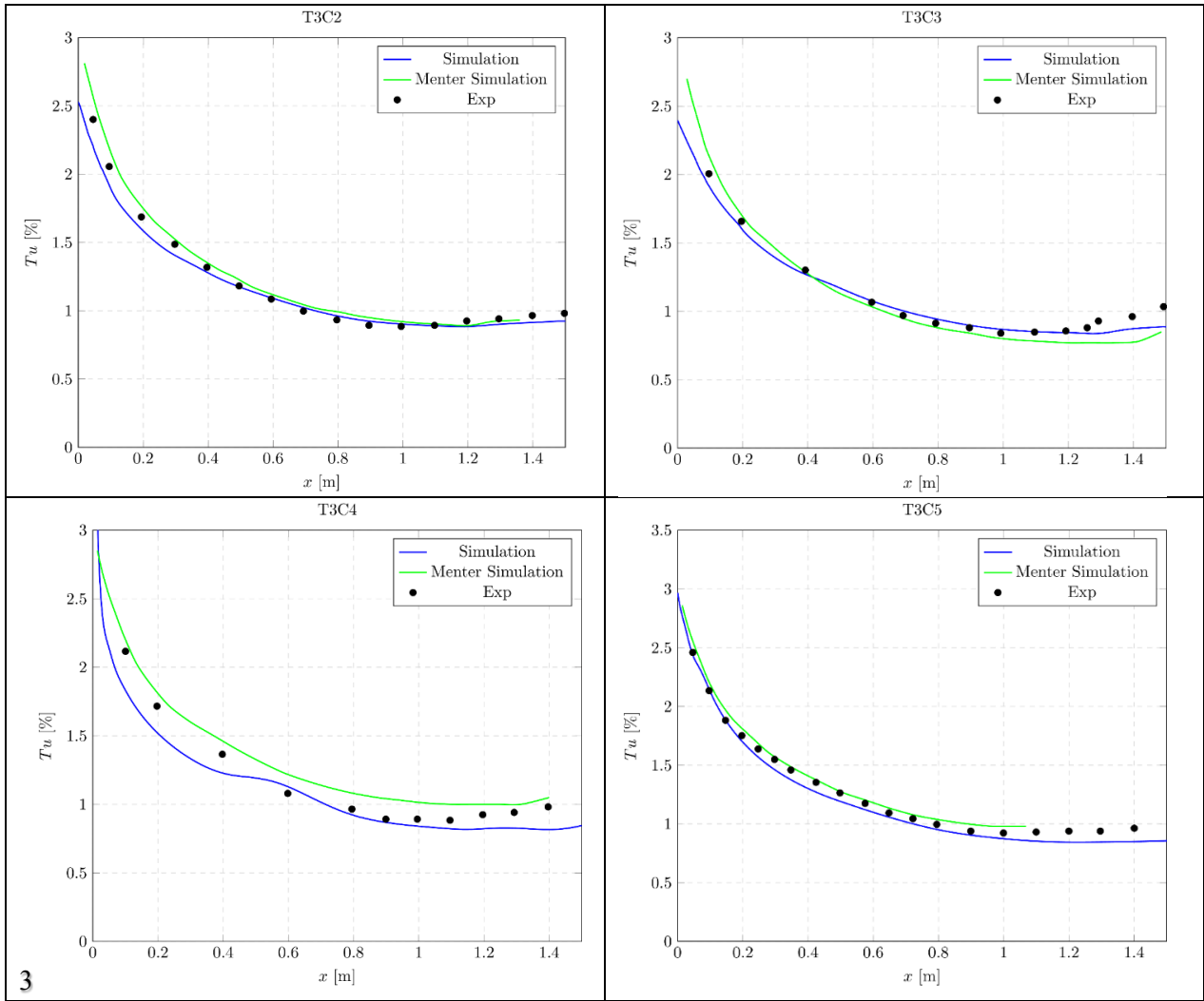


Figure 18: Turbulence intensity of T3C simulations. The numerical data is taken through a curve passing the centerline locations and obtained with the γ model.

Turbulence intensity profiles of T3C cases seem to be quite good. Skin friction coefficients for T3C2,

T3C3, T3C4 and T3C5 cases are presented in Figures 19-22.

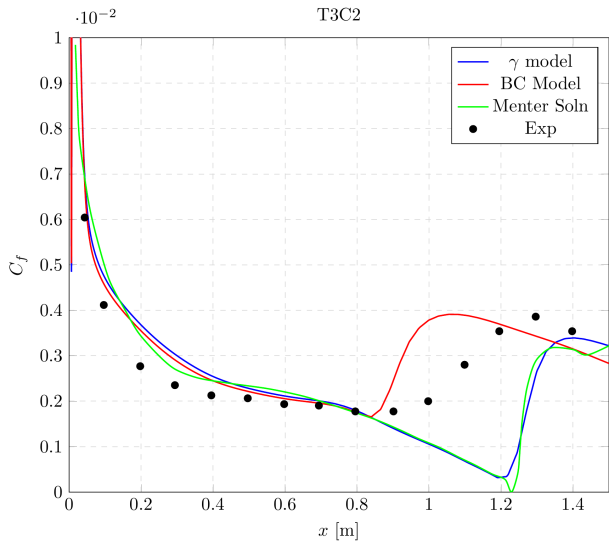


Figure 19: Skin friction coefficients obtained with Different Models for T3C2 Case

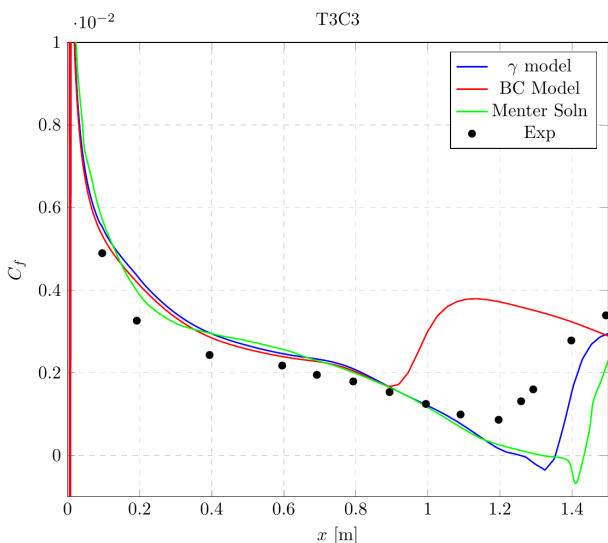


Figure 20: Skin friction coefficients obtained with Different Models for T3C3 Case

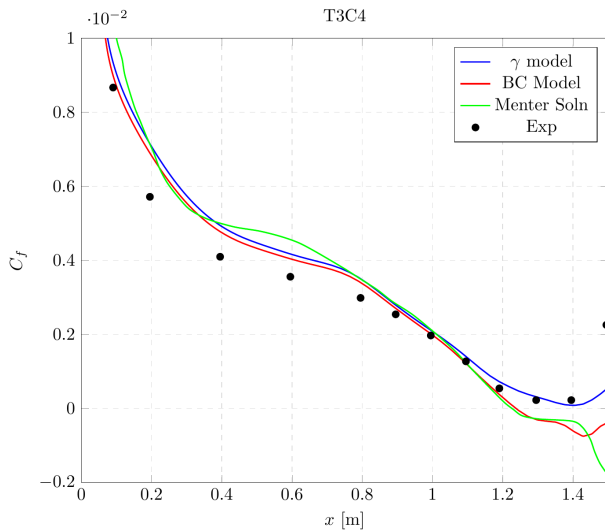


Figure 21: Skin friction coefficients obtained with Different Models for T3C4 Case

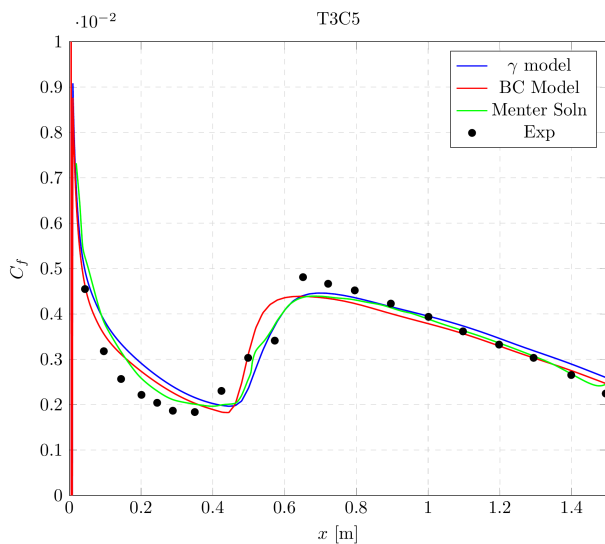


Figure 22: Skin friction coefficients obtained with Different Models for T3C5 Case

In the T3C2 case, both transition models capture transition onset with some errors. Both models predict a good enough skin friction coefficient after flow becomes fully turbulent. The Menter one-equation γ model and Bas-Cakmakciglu Model predict transition reasonably accurately in T3C3, similar to T3C2. T3C4 is the case with the smallest velocity. Although both models overpredict skin friction in the laminar region, they resolve transition onset accurately. Finally, in the T3C5 case, both transition models accurately resolve the laminar region, transition onset and length and flow after the transition. To sum up, the Menter one-equation γ model and the Bas-Cakmakciglu model predict transition onset and length similarly, and results

were reasonably accurate in favorable pressure gradient test cases.

Once again, T3C4 is the test case that is not well-suited for validation studies as in T3B. The transition onset is at the exit of the flat plate. Therefore, the results are open to experimental errors. The transition length is indefinite. Any differences in the transition onset estimations by the model may result in fully laminar flow results. Therefore, this test case is not a good test case for the evaluation of transition model performance.

2D Airfoil Cases

E387 Airfoil

Eppler E387 airfoil was tested to assess the γ model performance on 2D airfoil cases. Figure 23 shows the airfoil profile, which allows for a substantial amount of laminar flow before the transition on the suction side. Experimental data was taken from the study conducted at Langley low-turbulence pressure tunnel (LTPT) (McGhee (1988)) at Reynolds number 2×10^5 . Lift and drag coefficients at different angles of attack obtained in the experiments are available. The importance of this airfoil is that the laminar separation bubble is formed at the suction side, and flow re-attaches as turbulent. In other words, a separation-induced transition is observed at the E387 airfoil.

A 699×179 O-type grid with a 1.075 growth ratio is generated for simulations. The first layer thickness is assigned 1×10^{-5} units to the first cell to maintain $y^+ < 1$ and resolve the boundary layer accurately. Freestream turbulence intensity is specified as 0.18, and the viscosity ratio was chosen as 2. The computational grid used around the airfoil is given in Figure 24.

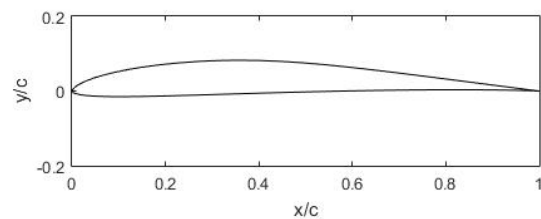


Figure 23: E387 airfoil profile

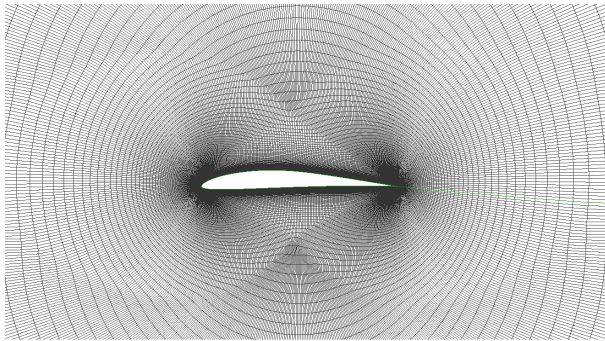


Figure 24: Computational domain around the E387 airfoil

In Figure 25, numerical results obtained with the γ model are compared with experimental data. This figure shows that the lift and drag coefficients obtained agree with experimental data, whereas a fully turbulent solution overpredicts the drag coefficients. The difference between the experimental data and simulation results at high angles of attack could be solver-based.

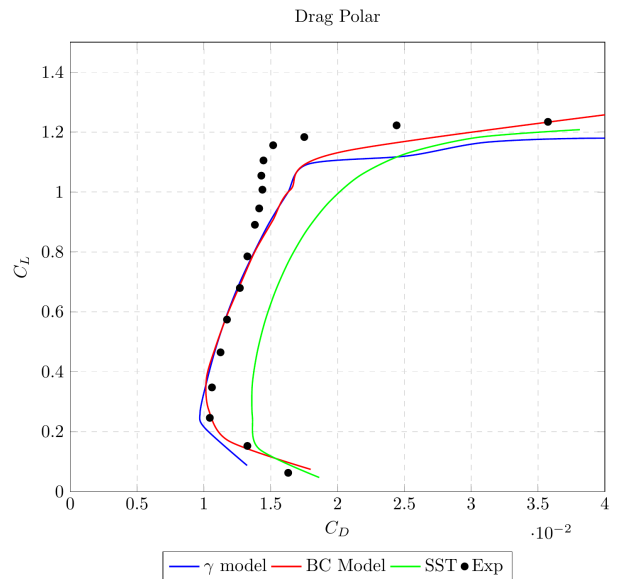


Figure 25: Drag polar of E387 airfoil

The importance of the E387 airfoil is that separation-induced transition occurs at the suction side of the airfoil. As expected, a fully turbulent solution misses the separation bubble. Both models predict that the flow separates to the laminar and reattaches as fully turbulent after the separation bubble.

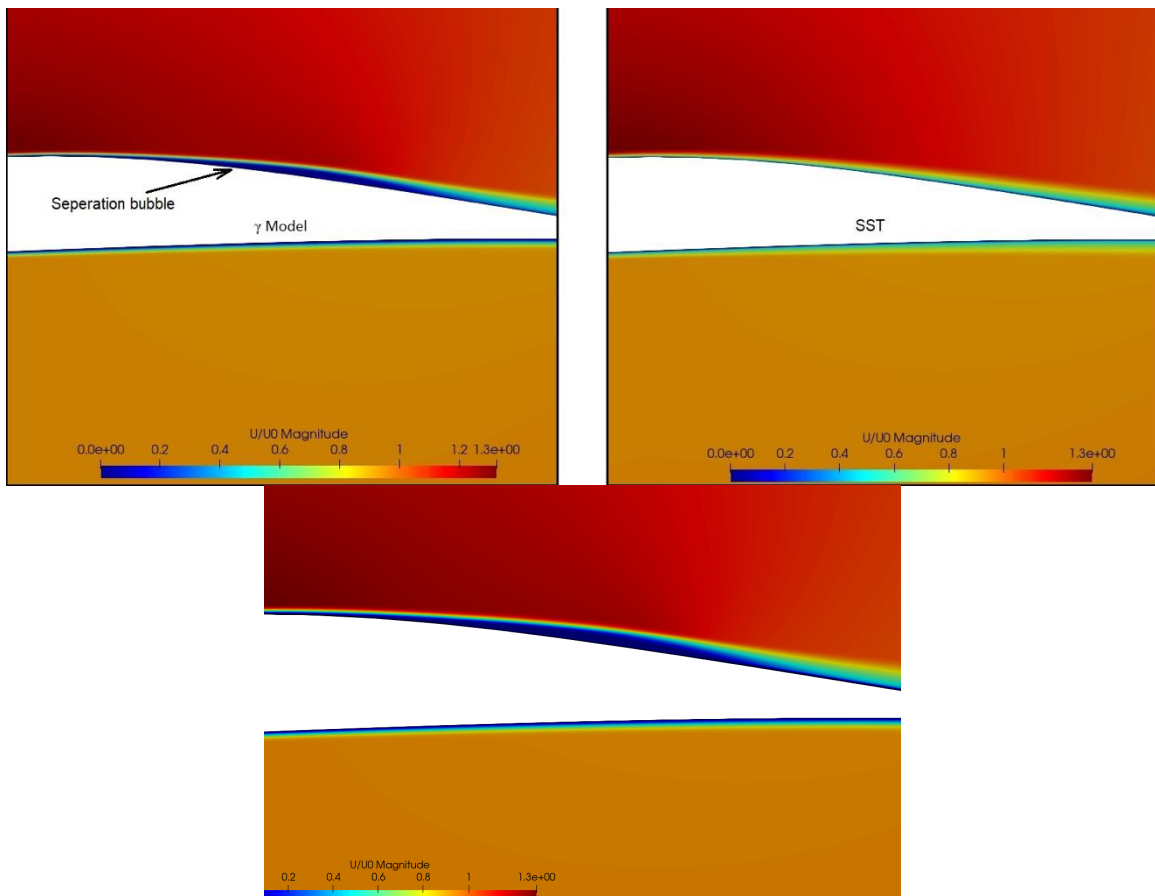


Figure 26: Flow field around the E387 airfoil top left: γ model, top right: SST, bottom: SA-BC model

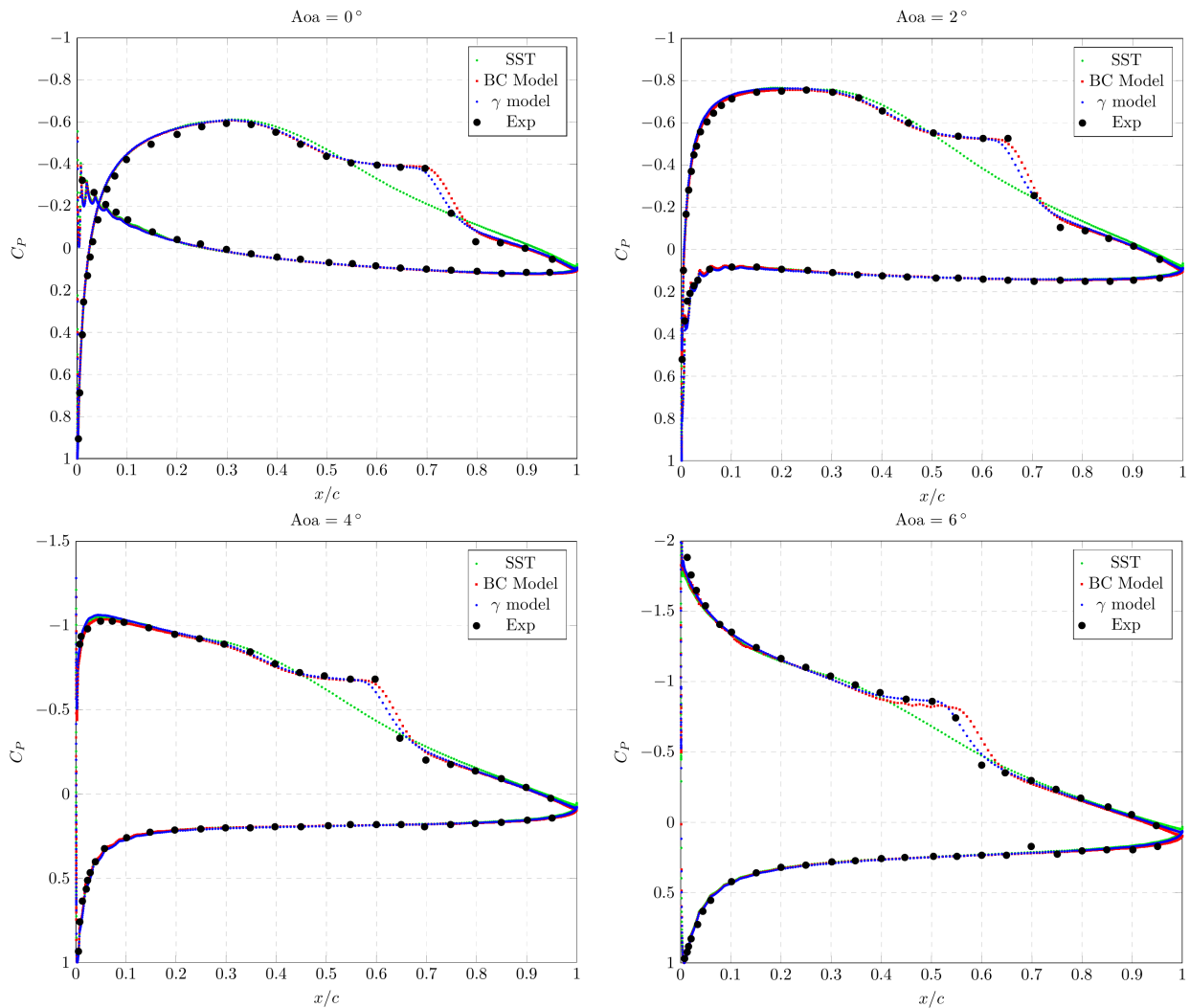


Figure 27: Comparison of Pressure Coefficients obtained with different models at different angles of attack

It can be inferred from Figure 26 that the γ model captures the separation bubble, whereas the fully turbulent solution based on the same model foundation (SST) misses it. The BC model also predicts a separation bubble at the same location with similar size. The same fact can be seen in Figure 27. The pressure coefficients obtained with the γ model, Bas- Cakmakcioglu model and SST are presented. Both transition models capture the separation-induced transition well enough, whereas a fully turbulent solution cannot. The reason for this difference stems from the lower skin friction estimations at the laminar forward part of the suction side. The adverse pressure gradient on the pressure side result in flow separation, according to von karmans momentum integral theory. The $k - \omega - SST$, on the other hand, model provide a higher fully turbulent skin friction that prevents the separation.

S809 Airfoil

The S809 airfoil is a laminar flow profile airfoil designed for horizontal axis wind turbine applications. Detailed experimental data, including drag coefficient, lift coefficient and pressure distribution of S809 airfoil, is available by Somers (1997). The airfoil profile is shown in Figure 28.

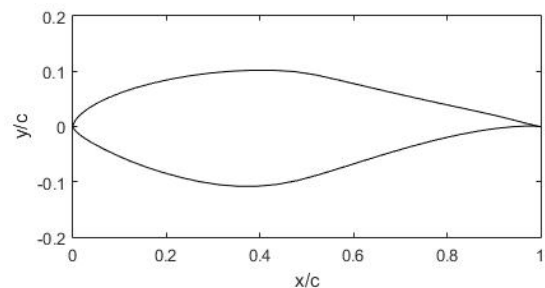


Figure 28: S809 airfoil profile

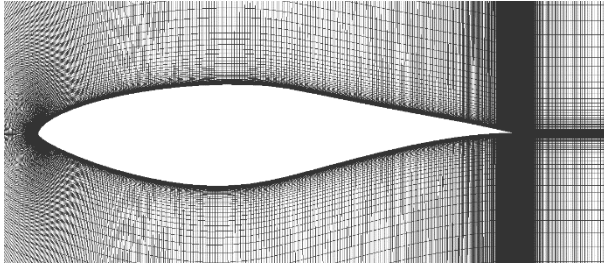


Figure 29: Computational domain around the S809 airfoil

C-type grid mesh is generated around the S809 airfoil with approximately 900 nodes (450 nodes on each side) around the airfoil. 100 nodes are created normal to airfoil profile with first layer thickness equal to 1×10^{-5} units to obtain $y^+ < 1$. The farfield boundary was located ten chord lengths from the airfoil. The computational domain used can be seen in Figure 29. Inlet conditions are given in Table 3.

Table 3: Inlet Conditions for the S809 Simulations

Case	Re_x	Mach	Chord (m)	FSTI(%)	μ_t/μ	α
S809	2×10^6	0.1	1	0.05	10	0° to 14°

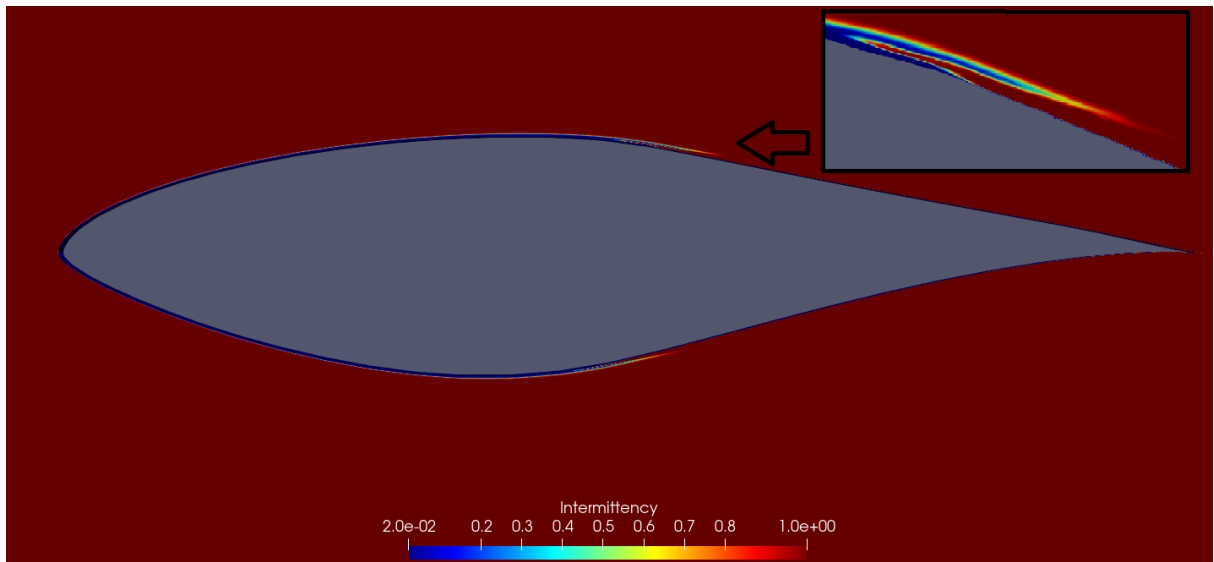


Figure 30: Intermittency at the angle of attack of $\alpha = 1^\circ$ obtained with the γ model.

The drag polar plots of the S809 airfoil at various angles of attacks are given in Figure 31. Transition models significantly improve the drag coefficient prediction since the effect of laminar flow over the airfoil surface is captured. Menter's one-equation γ model and the Bas-Cakmakcioglu model make similar predictions.

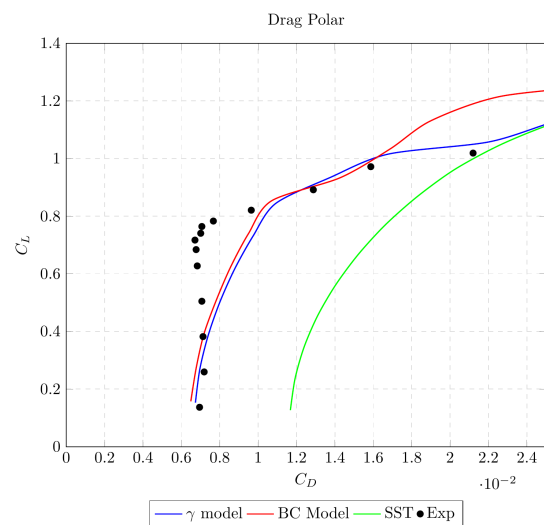


Figure 31: Drag polar of S809 Airfoil

Importance of Freestream Turbulence Properties

The most critical drawback of Menter's one equation γ model is its sensitivity to the inlet turbulence intensity and viscosity ratio, whose determination is the source of uncertainty. The model can predict different transition characteristics in transition onset and length for different inlet turbulence intensity and viscosity ratios.

The reasons for this behavior are the underlying turbulence model, $k - \omega - SST$, and the use of the local turbulence intensity in the implementation. The intermittency γ is coupled with the turbulent kinetic energy, hence the **local** turbulence intensity. Therefore γ model is affected by local turbulence characteristics. However, the success of the BC transition model shows that the turbulence intensity at the leading edge of the plate is the critical factor for the transition onset. Notice that the underlying turbulence model of the BC transition model, Spalart-Allmaras, does not provide any turbulence intensity information.

On the other hand, in external flow simulations, a user must provide appropriate k and ω boundary conditions at the freestream to solve transitions accurately. The k can be determined relatively easily. However, it is challenging to determine ω in engineering problems. Moreover, the freestream parameters decay until the leading edge, making applying these parameters even more difficult. To show this dependence on freestream conditions, the Menter one-equation γ model is tested for different freestream turbulence properties T3A test case.

Note that the freestream turbulence intensity alters the transition onset, and this parameter is measured and reported for all test cases. Therefore, the freestream turbulence intensity is kept the same with the experimental data while the viscosity ratio changes. Applied freestream turbulence properties are presented in Table 4.

Table 4: Inlet viscosity ratio applied in tests

	μ_t/μ						
Setup	1	4	9	12	30	60	120

The response of Menter one equation γ model to different viscosity ratios is given in Figure 32.

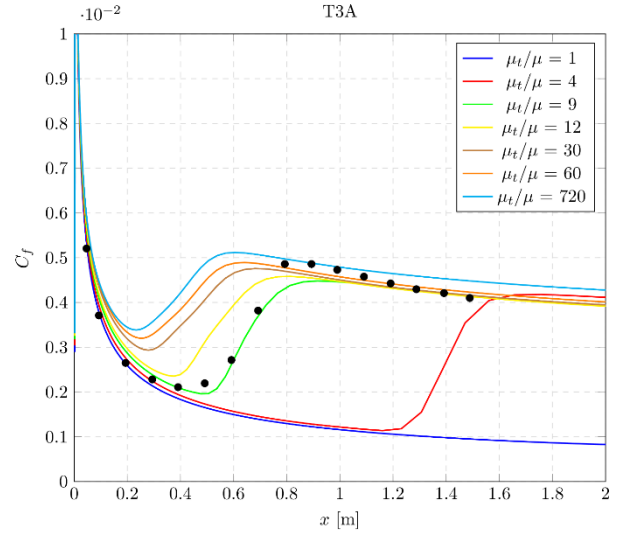


Figure 32: Effect of the viscosity ratio of freestream inlet conditions

Figure 32 shows that the freestream viscosity ratio significantly affects the results. For $\mu_t/\mu = 1$, flow behaves completely laminar. An increase in the viscosity ratio results in the transition onset location moving closer to the leading edge of the plate.

Discussion

In this study, we have tested two transition models a natural transition, bypass transition with and without pressure gradient and separation-induced transition. Both models can predict natural transition accurately and bypass transition with reasonable accuracy. Zero pressure gradient test case simulations show that the success of the γ model is highly dependent on the freestream turbulence properties. It should be noted that some of the freestream turbulence characteristics are difficult to determine in real-life applications. The study showed that transition prediction could change significantly for different viscosity ratio specifications. Mentioned deficiency complicates the simulation preparation and, as a result, the applicability of the γ model to general flow cases. BC transition model does not suffer such a shortcoming.

Zero-equation Bas-Cakmakcioglu transition model predicts transition effects similar to the γ model for different transition modes. On the other hand, the BC transition model does not suffer excessive turbulence boundary conditions requirements as it only requires the freestream turbulence intensity. In addition to that, as it does not solve additional differential equations, solutions are obtained faster

compared to the γ model. It should be noted that both models predict the transition onset accurately, and both of them can be applied depending on the selection of the underlying turbulence model.

CONCLUSIONS

In this study, we have studied the Menter one-equation γ and Baş-Çakmakçioğlu models for transitional flows. The models are implemented in our open-source CFD solver. Then, the transition model is tested on different well-known benchmark transitional cases. Results show that both transition models give similar predictions as long as freestream turbulence properties are specified accurately. The performance of both transition models used in this study depends on the freestream turbulence intensity. BC transition model stands out as it does not suffer from the freestream viscosity ratio.

Both models are tested in this study on several flat-plate and two-dimensional airfoil cases. None of the test cases were decisive for the model performance for relaminarization problems. We recommend Baş-Çakmakçioğlu model for external aerospace applications since it is simpler to implement, cheaper to run, and easier to apply than γ model.

As discussed previously, the transition onset depends on the freestream turbulence. This fact is shown by various experiments, including Schubauer, ERCOFTAC, Sinclair, and Fashifar experiments, as shown in Figure 3. The turbulence intensity is a local parameter in k -based turbulence models. Therefore, such models use local k as the transition trigger measure. These models include Menter's γ and $\gamma - Re_{\theta c}$ model and Walter and Colkijat's $k_L - k_T - \omega$ models.

However, this selection brings about a disadvantage to k -based methods. The freestream k that is supplied as a boundary condition decays significantly in the free stream. The decay rate of the k in all $k - \omega$ models is given as

$$D_k = -\beta^* \rho \omega k \quad (21)$$

This indicates that the decay rate of k (hence Tu) depends on both k and ω . Therefore, local turbulence intensity is affected by both parameters. This is also true for γ model since the modified decay rate given in Equation 16 allows the decay of k even within the laminar region.

On the other hand, the experiments do not indicate any correlation between the local turbulence intensity and the transition onset. We have tested two different transition models for this purpose. The first one is $k - \omega$ -based Menter's γ model, in which the turbulent decay is an issue. The other one is the SA-based BC transition model, where local turbulence intensity (hence decay of Tu) is not available, and the freestream Turbulence intensity is supplied as a parameter.

The numerical experiments show that for a wide range of freestream turbulence, the SA-BC transition model provides excellent results without any Tu -decay. The γ models also exhibit good results, provided that the free stream ω is supplied as μ_t such that k -decay is also fit. However, ω is not available for the free stream. Most CFD codes assign a small default ω at the free stream boundaries. Therefore, the decay rate at the freestream becomes small.

The requirement of the ω Boundary condition brings a couple of problems. If the flow is external, the user should adjust the freestream k at the leading edge of the solid boundary to fit the freestream k . For internal flows, such as turbomachinery flows, the decay rate of the high-turbulence intensity flows becomes important in k -based model.

Similar problems are implied in Menter's original work. ERCOFTAC cases (which are more akin to internal flow due to the pressure change) provide the turbulence decay data. Therefore, the freestream ω is adjusted for all test cases. The γ model is calibrated with these test cases with both freestream k and ω . Therefore simulation results on these calibration test cases are suitable.

On the other hand, The BC transition model fits the results comparably without turbulence decay and using only the freestream turbulence intensity. Therefore, we can argue that the local turbulence intensity has little to no effect on the transition onset, as the experiments suggest. Therefore utilization of the local turbulence feature in k -based transition models brings unjustified complexity.

We have demonstrated the dependency of the k -based models in the freestream turbulence parameters. As seen in the results, we have altered the freestream turbulent viscosity within the range of flat plate μ_t of Menter's simulations. It is seen that this parameter has a significant effect on the transition onset calculations. Although it is not given in this study, the W&C model shows similar

results. We can conclude that available $k - \omega$ -based transition models have a similar shortcoming.

Another feature of the γ model is that the transition length is also calibrated in the models. The BC transition model is an abrupt transition model. However, the tests show that both models show similar transition lengths in all flat plate tests. We can conclude that all available transition experiments transition is abrupt, and transition length calibrations require more experimental data.

As the second claim of Menter was that the γ model could also be used in relaminarization problems and separation-induced transition problems. We could not find experimental data for relaminarization to

test the former. For the latter, we have tested two airfoils. Both γ and BC transition models exhibit similar results. Drag polars show that the BC transition model has a small edge over the γ model without adjusting the free stream turbulent viscosity. Therefore we can argue that the BC transition model is ready for the external transient flow conditions without adjustment.

It should be noted that it is relatively easy to apply the γ model in external flow calculations. The difficulties mentioned above may arise in internal flow transition problems. We left the internal flow simulations as future work.

LIST OF SYMBOLS

BC	Bas Cakmakcioglu (Transition Model)
CFD	Computational Fluid Dynamics
DNS	Direct Numerical Simulation
FVM	Finite Volume Method
LES	Large Eddy Simulation
RANS	Reynolds Averaged Navier Stokes
SA	Spallart Allmaras
SST	Shear Stress Transport
WCM	Walters Cokljat Model
E	Destruction Term
ν	Kinematic Viscosity
μ	Dynamic Viscosity
P	Production Term
Re_ν	Vorticity Reynolds Number
Re_{θ_c}	Critical Momentum Thickness Reynolds Number
Re_{θ_t}	Transition Onset Momentum Thickness Reynolds Number
Re_θ	Momentum Thickness Reynolds Number
Re	Reynolds Number
S	Strain Rate Magnitude
μ_T	Turbulent viscosity
Tu	Turbulence Intensity
Ω	Vorticity Magnitude
γ	Intermittency
k_L	Laminar Kinetic Energy
k	Turbulent Kinetic Energy
λ	Pressure Gradient Parameter
ω	Specific Turbulence Dissipation Rate
ρ	Density

REFERENCES

Bas, Onur, Cakmakcioglu, Samet C, & Kaynak, Unver. 2013. A novel intermittency distribution-based transition model for low-re number airfoils.

Page 2531 of: 31st AIAA applied aerodynamics conference.

Cakmakcioglu, Samet C, Bas, Onur, Mura, Riccardo, & Kaynak, Unver. 2020. A revised one-equation transitional model for external aerodynamics. Page 2706 of: AIAA Aviation 2020 Forum.

Cakmakcioglu, Samet Caka, Bas, Onur, & Kaynak, Un- ver. 2018. A correlation-based algebraic transition model. Proceedings of the Institution of Mechanical Engineers, Part C: Journal of Mechanical Engineering Science, 232(21), 3915–3929.

Cho, Ji Ryong, & Chung, Myung Kyoan. 1992. A $k-\epsilon-\gamma$ equation turbulence model. Journal of Fluid Mechanics, 237, 301–322.

Dhawan, SJ, & Narasimha, R. 1958. Some properties of boundary layer flow during the transition from laminar to turbulent motion. Journal of Fluid Mechanics, 3(4), 418–436.

Dikbaş, E, and Baran ÖU. 2022, Implementation, verification and assessment of vortex capturing capabilities of k-kl turbulence model., Isı Bilimi ve Tekniği Dergisi 42 (1), 113-122.

Duru, C, Alemdar H, and Baran ÖU. 2021 CNNFOIL: Convolutional encoder decoder modeling for pressure fields around airfoils., Neural Computing and Applications 33 (12) 6835-6849.

Emmons, Howard W. 1951. The laminar-turbulent transition in a boundary layer-Part I. Journal of the Aeronautical Sciences, 18(7), 490–498.

- Frei, Walter. 2013. Which Turbulence Model Should I Choose for My CFD Application? URL <https://www.comsol.com/blogs/which-turbulence-model-should-choose-cfd-application/>. accessed (2023): 03-20.
- Jones, W Poo, & Launder, BrnE. 1973. The calculation of low-Reynolds-number phenomena with a two-equation model of turbulence. *International Journal of Heat and Mass Transfer*, 16(6), 1119–1130.
- Kaynak, Unver, Bas, Onur, Cakmakcioglu, Samet Caka, & Tuncer, Ismail Hakki. 2019. Transition modeling for low to high speed boundary layer flows with CFD applications. In: *Boundary layer flows-theory, applications and numerical methods*. intechopen.
- Langtry, Robin B, & Menter, Florian R. 2009. Correlation-based transition modeling for unstructured parallelized computational fluid dynamics codes. *AIAA journal*, 47(12), 2894–2906.
- Langtry, Robin Blair. 2006. A correlation-based transition model using local variables for unstructured parallelized CFD codes.
- Langtry, Robin Blair, Menter, FR, Likki, SR, Suzen, YB, Huang, PG, & Völker, S. 2006b. A correlation-based transition model using local variables—part II: test cases and industrial applications.
- Mayle, RE, & Schulz, A. 1996. The path to predicting bypass transition. Page V001T01A065 of: *Turbo Expo: Power for Land, Sea, and Air*, vol. 78729. American Society of Mechanical Engineers.
- Mayle, Robert Edward. 1991. The 1991 IGTI scholar lecture: the role of laminar-turbulent transition in gas turbine engines.
- McGhee, Robert J. 1988. Experimental results for the Eppler 387 airfoil at low Reynolds numbers in the Langley low-turbulence pressure tunnel. Vol. 4062. National Aeronautics and Space Administration, Scientific and Technical. 55
- Menter, Florian R. 1994. Two-equation eddy-viscosity turbulence models for engineering applications. *AIAA journal*, 32(8), 1598–1605.
- Menter, Florian R, Kuntz, Martin, & Langtry, Robin. 2003. Ten years of industrial experience with the SST turbulence model. *Turbulence, heat and mass transfer*, 4(1), 625–632.
- Menter, Florian R, Langtry, Robin Blair, Likki, SR, Suzen, YB, Huang, PG, & Völker, S. 2006a. A correlation-based transition model using local variables—part I: model formulation.
- Menter, Florian R, Smirnov, Pavel E, Liu, Tao, & Avancha, Ravikanth. 2015. A one-equation local correlation-based transition model. *Flow, Turbulence and Combustion*, 95(4), 583–619.
- Menter, FR, & Langtry, RB. 2012. Transition Modelling for Turbomachinery Flows. *Low Reynolds Number Aerodynamics and Transition*, 31–58.
- Menter, FR, Esch, T, & Kubacki, S. 2002. Transition modelling based on local variables. Pages 555–564 of: *Engineering Turbulence Modelling and Experiments 5*. Elsevier.
- Menter, FR, Langtry, R, & Völker, S. 2006b. Transition modelling for general purpose CFD codes. *Flow, turbulence and combustion*, 77(1), 277–303.
- Nichols, Robert H. 2010. *Turbulence models and their application to complex flows*. University of Alabama at Birmingham, Revision, 4, 89.
- Savill, AM. 1993. Some recent progress in the turbulence modelling of bypass transition. *Near-wall turbulent flows*, 829–848.
- Schubauer, Galen B, & Klebanoff, Philip S. 1955. *Contributions on the mechanics of boundary-layer transition*. Tech. rept.
- Smith, Apollo Milton Olin. 1956. *Transition, pressure gradient and stability theory*. Douglas Aircraft Co., Report ES 26388.
- Somers, Dan M. 1997. Design and experimental results for the S809 airfoil. Tech. rept. National Renewable Energy Lab.(NREL), Golden, CO (United States).
- Steelant, Johan, & Dick, Erik. 2001. Modeling of laminar- turbulent transition for high freestream turbulence. *J. Fluids Eng.*, 123(1), 22–30.
- Suzen, Y, & Huang, P. 2000. An intermittency transport equation for modeling flow transition.

Page 287 of: 38th Aerospace Sciences Meeting and Exhibit. 57

Walters, D Keith, & Cokljat, Davor. 2008. A three-equation eddy-viscosity model for Reynolds-averaged Navier–Stokes simulations of transitional flow. *Journal of fluids engineering*, 130(12).

Wang, Jiang-Sheng, & Wang, Jin-Jun. 2021. Wake-induced transition in the low-Reynolds-number flow over a multi-element airfoil. *Journal of Fluid Mechanics*, 915.